

Photoabsorption and fluorescence excitation of malononitrile in the vacuum UV region

S. Uchida^a, K. Tabayashi^a, M. Tanaka^a, O. Takahashi^a, K. Saito^a, M. Kono^b,
T. Ibuki^b

^a Department of Chemistry, Hiroshima University, Kagamiyama, Higashi-Hiroshima 739, Japan

^b Institute for Molecular Science, Myodaiji, Okazaki 444, Japan

Received 25 November 1996; in final form 30 September 1997

Abstract

The cross-sections for the photoabsorption and fluorescence excitation of $\text{CH}_2(\text{CN})_2$ were measured in the 105–200 nm region using synchrotron radiation. The absorption bands were interpreted in terms of the transitions to the valence and Rydberg states. The vibrational progressions observed in the Rydberg bands were assigned on the basis of ab initio MO calculations. $\text{CN}(\text{B}^2\Sigma^+)$ and $\text{CN}(\text{A}^2\Pi_1)$ photofragments were identified by a dispersed fluorescence spectrum. The fluorescence quantum yields for $\text{CN}(\text{B}^2\Sigma^+)$ and $\text{CN}(\text{A}^2\Pi_1)$ formation increase with decreasing excitation wavelengths. The $\text{CN}(\text{B}^2\Sigma^+)$ quantum yield has a maximum of 0.85% at 107 nm. © 1998 Elsevier Science B.V.

1. Introduction

Photochemistry of simple mono-cyanides, RCN ($\text{R} = \text{H}, \text{Br}, \text{I}, \text{CH}_3$ and CF_3) has been studied extensively in the VUV region, where fluorescent photofragments, $\text{CN}(\text{A}^2\Pi_1)$ and $\text{B}^2\Sigma^+$, have been detected. Using synchrotron radiation as a VUV excitation source, the absorption and fluorescence cross-sections for these cyanides [1–9] have been determined against the wavelength of the exciting light. The fluorescence quantum yields obtained from the cross-sections are no greater than 0.4, indicating that non-radiative decay channels are significant upon excitation by VUV photons at energies up to 12 eV (~ 100 nm). The fluorescence measurements, however, give us abundant information about the dynamics in the dissociative excitation channels and their

interactions with other possible product decay channels from the VUV photoexcited states. Fluorescence polarization measurements [1,3–5] have provided the details on the lifetimes and the characteristics of the photoexcited states. The deuterium isotope enhancement observed in the fluorescence quantum yield of CH_3CN [1,7,8] has been explained as due to the competition of the dissociative excitation process with fast non-radiative reaction processes.

We have now measured the absorption and fluorescence cross-sections of $\text{CH}_2(\text{CN})_2$ to understand its excited state dynamics in comparison with those of CH_3CN . The only study related to this subject is a measurement of electron-impact excitation [10] where the 5–13 eV bands were tentatively assigned to the valence and Rydberg transitions based on the similarity of the electron impact spectrum to that of

HCN. No other electronic excitation data except for photoelectron spectra [11,12] have been reported. The present Letter describes quantitative measurements of the photoabsorption and dissociative (fluorescence) excitation cross-sections and the quantum yields for the dissociative excitation processes. The quantum yields for the CN(A) and CN(B) formation are separately determined.

2. Experiment and procedure

The VUV photoabsorption and fluorescence measurements of $\text{CH}_2(\text{CN})_2$ were carried out on the BL2A beamline at the ultraviolet synchrotron orbital radiation (UVSOR) facility of the Institute for Molecular Science (IMS). The details of the experimental arrangement and procedure have been described previously [1]. Synchrotron radiation was dispersed by a 1 m Seya monochromator (Hitachi SNM-2) and introduced into a gas cell through an LiF window. The uncertainty in the monochromator wavelength was estimated to be ± 0.03 nm. The gas cell with an optical path length of 27.3 cm was newly designed to control the cell temperature, so that spectroscopic measurements of the sample with low vapor pressure could be made at elevated temperatures. For absorption and fluorescence excitation measurements, the intensities of the primary excitation beam transmitted and the fluorescence from the gas cell were recorded simultaneously against the excitation VUV wavelength. In the measurement of dispersed fluorescence spectra, a 0.32 m monochromator (JY-HR320) was installed at the fluorescence observation port of the cell. The sample with stated purity of $\geq 99.0\%$ was purchased from Tokyo Chemical Ind. Co. Ltd., and volatile impurities were degassed under vacuum.

In order to support the analysis of the Rydberg transitions and vibrational progressions observed in the VUV absorption spectra, ab initio MO calculations were carried out for the ground and ionic states of $\text{CH}_2(\text{CN})_2$. Ionic states were chosen to approximate the geometries and vibrational structures of relevant Rydberg states with the same ionic core. The geometries and vibrational frequencies were determined at the HF level with the 6-31G** basis set using the GAUSSIAN 92 programs [13]. The ge-

ometries were fully optimized using analytical gradient procedures, and the vibrational frequencies were obtained by numerical differentiation of the energy gradient. Thermochemical MO calculations were also performed for several species using the G2 procedure [14].

3. Results and discussion

3.1. Photoabsorption spectrum and rydberg assignments

Since this molecule has C_{2v} symmetry [15] (Fig. 1), the electronic configuration of the outer valence shells can be expressed as $(4a_1)^2(3b_2)^2(1a_2)^2(5a_1)^2(4b_2)^2(2b_1)^2$ under the HF MO formalism [16]. The ionization energies E_1 of these orbitals have been determined [12] to be 14.06, 13.91, 13.59, 13.42, 13.14 and 12.72 eV, respectively. The outermost four orbitals, $2b_1-1a_2$, have π_{CN} character with interactions within the four π_{CN} of the two CN groups and the $4a_1$ and $3b_2$ orbitals have n_{CN} character [16].

Fig. 2 shows the photoabsorption (solid line) and fluorescence excitation (dotted line) cross-sections in the range of 105–150 nm, obtained with a resolution of 0.2 nm at the gas cell temperature of 45°C. In the

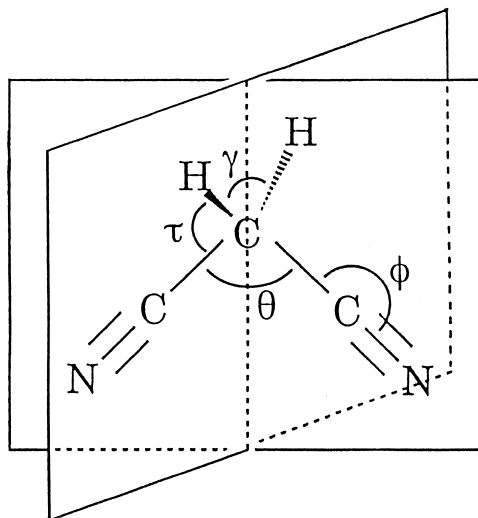


Fig. 1. Schematic molecular conformation and structural parameters of $\text{CH}_2(\text{CN})_2$.

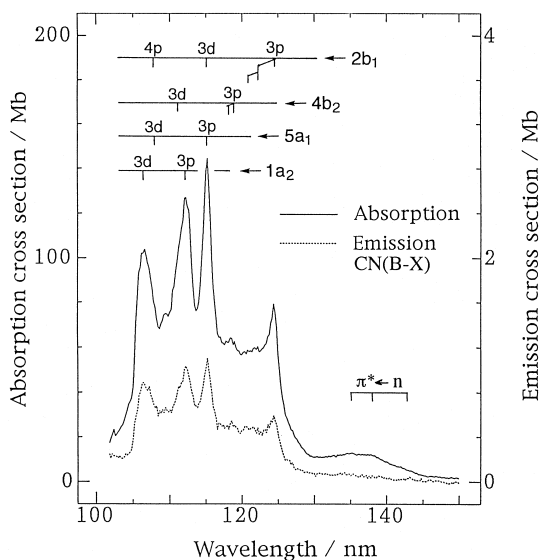


Fig. 2. Absorption cross-section of $\text{CH}_2(\text{CN})_2$ and fluorescence excitation cross-section for $\text{CN}(\text{B})$ formation vs. wavelength of exciting light in the 105–150 nm region. Sample pressure was 15 mTorr.

150–200 nm range, no apparent signals above the noise level were detected for either the photoabsorption or the fluorescence excitation spectra. The strongest peak in the absorption has a cross-section of ≥ 100 Mb; the magnitude is comparable with those of other cyanides [2,6] with π_{CN} electrons in the highest occupied MO. The absorption cross-section was examined at several sample pressures from 5 to 30 mTorr (1 Torr = 133.3 Pa), where the absorbance $\ln(I_0/I)$ was linearly dependent on the gas pressure. The uncertainty in the reduced cross-section is estimated to be less than $\pm 15\%$ of the given value.

Our assignments of the photoabsorption bands are based on the term value consideration [17] using the Rydberg formula,

$$h\nu = E_i - \frac{R}{(n - \delta)^2}, \quad (1)$$

where R , n and δ are the Rydberg constant, principal quantum number and quantum defect, respectively.

The broad diffuse bands at 134.8, 137.8 and 142.5 nm have term values of $\geq 28400 \text{ cm}^{-1}$ with respect to the lowest E_i of 12.72 eV, although they are

superimposed with each other in the 130–140 nm range. They are assigned to the intervalence transitions. Rianda et al. have attributed the 130–140 nm bands in their electron-impact spectra to the $\pi^* \leftarrow n_{\text{CN}}$ transitions [10]. As with electron-impact excitation, no clear evidence for the transitions of the valence shell electrons to the ns Rydberg states is found. The peaks in the shorter wavelengths, < 130 nm, are assigned to the Rydberg transitions converging to the lowest four ionization limits at 12.72, 13.14, 13.42 and 13.59 eV. Their term values calculated are grouped into two, 20500–22500 and 15500–15800 cm^{-1} , which suggests that the upper Rydberg states may be the 3p and 3d orbitals, respectively. Table 1 summarizes the photoabsorption bands and our Rydberg assignments. The Rydberg transitions ($3p \leftarrow 2b_1$, $3p \leftarrow 4b_2$) of the π_{CN} orbitals have been found to be accompanied by vibrational progressions with energy spacings of ≈ 1450 and $\approx 500 \text{ cm}^{-1}$. The quantum defects of the π_{CN} electrons to the np and nd orbitals are found to be 0.73 ± 0.05 and 0.37 ± 0.02 , which can be compared with the reported values, $\delta(np) = 0.69 \pm 0.07$ and $\delta(nd) = 0.32 \pm 0.02$, respectively, for the similar $np \leftarrow \pi_{\text{CN}}$ and $nd \leftarrow \pi_{\text{CN}}$ transitions [18] in CH_3CN .

In order to examine the change in the molecular structure upon excitation to the $(2b_1)^{-1}$ Rydberg states, the geometries of the ground and ionic states were optimized at the HF level. The geometric parameters (Fig. 1) of the first ionic state,

Table 1
Rydberg assignments for the photoabsorption bands of $\text{CH}_2(\text{CN})_2$

Band peak (nm)	Assignment	Term value (cm^{-1})	$\Delta\nu$ (cm^{-1})	δ
124.4	$3p \leftarrow 2b_1$	22208		0.78
122.2	$+1\nu_3$		1447	
120.8	$+1\nu_3 + 2\nu_5$		2×474	
118.9	$3p \leftarrow 4b_2$	21554		0.76
118.2	$+1\nu_5$		498	
115.2	$3d \leftarrow 2b_1$	15788		0.36
	$3p \leftarrow 5a_1$	21434		0.74
112.4	$3p \leftarrow 1a_2$	20603		0.69
111.2	$3d \leftarrow 4b_2$	15731		0.39
109.5	$3p \leftarrow 3b_2$	20706		0.71
108.0	$4p \leftarrow 2b_1$	9679		0.69
	$3d \leftarrow 5a_1$	15647		0.35
106.6	$3d \leftarrow 1a_2$	15802		0.37

Table 2
Geometrical parameters of CH₂(CN)₂

Equilibrium conformation	r_{C-C} (Å)	$r_{C=N}$ (Å)	r_{C-H} (Å)	θ (°)	ϕ (°)	τ (°)	γ (°)
ground state (\tilde{X}^1A_1)							
obs. ^a	1.468	1.167	1.088	109.4	176.3	108.7	–
RHF/6-31G**	1.471	1.133	1.083	112.3	178.5	109.1	108.1
ionic state ($2b_1$) ⁻¹ \tilde{X}^2B_1							
UHF/6-31G**	1.462	1.176	1.083	83.3	187.8	113.7	114.9

^aCalculated from MW measurements; see Ref. [15].

($2b_1$)⁻¹ \tilde{X}^2B_1 , by the UHF/6-31G** calculation are compared with the RHF/6-31G** values for the ground state, \tilde{X}^1A_1 (Table 2) along with those observed [15] for the ground state. The molecular geometries of the ionic state change significantly from those of the ground state: the bond angle θ (< CCC) is smaller by 29° and τ (< HCH) larger by 7° than in the ground state. Mulliken's population analysis [19] shows that the removal of the $\pi(2b_1)$ electron reduces the excess negative charge distributed on the two N atoms and increases the positive charges on the two H atoms. The reduction of the negative charges on the N atoms weakens their repulsive interaction and enhances the in-phase π - π interaction between the two CN groups, which explains the significant change in θ (< CCC) from that in the ground state. The change in τ (< HCH) may also be ascribed to that in the repulsive interaction between the terminal H atoms. The large change in the equilibrium geometries upon excitation to the Rydberg state induces vibrational excitation of the associated vibrational modes. The observed vibrational progressions are hence assigned to the CH₂ scissors $\nu_3(a_1)$ and CCC deformation $\nu_5(a_1)$ modes.

To confirm the vibrational spacings, a vibrational frequency analysis was also performed on the ($2b_1$)⁻¹ Rydberg member using the 6-31G** basis set. It is well known that the harmonic frequencies calculated at the HF level are generally 10–15% higher than the observed values. The corrections for the deficiencies in the theory and the neglect of vibrational anharmonicity have usually been accomplished by introducing a scaling factor. A scaling factor of $r_s = 0.89$ – 0.90 has been chosen as the average of the ratio $\nu_{\text{expt}}/\nu_{6-31G^*}$ for a large number of vibrational frequencies [19,20]. In going from the 6-31G* to the

6-31G** basis set, we believe that there is no need for a substantial change in the correction factor. Here, the (U)HF/6-31G** frequencies are scaled with $r_s = 0.90$ and used for the prediction of the relevant vibrational frequencies. The present vibrational analysis for the ionic ($2b_1$)⁻¹ \tilde{X}^2B_1 state gives the scaled frequencies of $\nu_3(a_1) = 1395$ and $\nu_5(a_1) = 482$ cm⁻¹, which are found to be consistent with the observed values, ≈ 1450 and ≈ 500 cm⁻¹.

3.2. Fluorescence measurements and fluorescence quantum yields

In a separate measurement of the dispersed fluorescence spectra, CN(A²Π_i-X²Σ²) and CN(B²Σ⁺-X²Σ⁺) emissions were identified when CH₂(CN)₂ was excited at the intense photoabsorption peaks of 124.4 and 115.2 nm. No other fragment emission was discernible in the UV and visible wavelengths. The dissociative excitation,



was thus confirmed as the prominent fluorescent decay channel following the VUV excitation of CH₂(CN)₂.

In the measurement of the fluorescence excitation spectra, the emission intensities from the CN(A-X) and CN(B-X) bands were separately detected with the combinations of an optical filter and a PMT, i.e. (Toshiba C39A + Hamamatsu R585) and (Toshiba O54 + Hamamatsu R955). Each fluorescence excitation cross-section was determined by comparing the photoemission intensity with that of the reference molecule, CH₃CN, for which the absolute values have been determined [7,8]. The fluorescence excitation cross-section shown in Fig. 2 is thus obtained

Table 3
G2 energies (in hartree)

Species	$E_0(\text{G2})$
$\text{CH}_2(\text{CN})_2$	-224.623199
CH_3CN	-131.869531
CN	-92.582761

for the CN(B–X) transition. Most of the band peaks in the absorption are reproduced in the fluorescence excitation spectrum. The CN(A) excitation spectrum is not presented, since the spectral pattern is similar to that observed for the CN(B) excitation.

The onset wavelength to generate the CN(B) state was found to be 147.5 nm, which corresponds to the bond dissociation energy, $D_0(\text{H}_2(\text{CN})\text{C}-\text{CN}) \leq 5.21$ eV when the excitation energy [21] of the CN(B) is used. The value is compared with $D_0(\text{H}_2(\text{CN})\text{C}-\text{CN}) = 4.65$ eV calculated from the total electronic energies of the parent and fragment species based on the G2 procedure, which was shown to predict the values to within ± 0.1 eV [14]. The G2 energies are listed in Table 3. By adoption of the G2 values, the energy difference between the observed and predicted values indicates that the exit potential surface leading to $\text{CH}_2\text{CN} + \text{CN}(\text{B})$ has a repulsive nature and the excess energy of ≈ 0.5 eV might have been partitioned into the translation between the fragments.

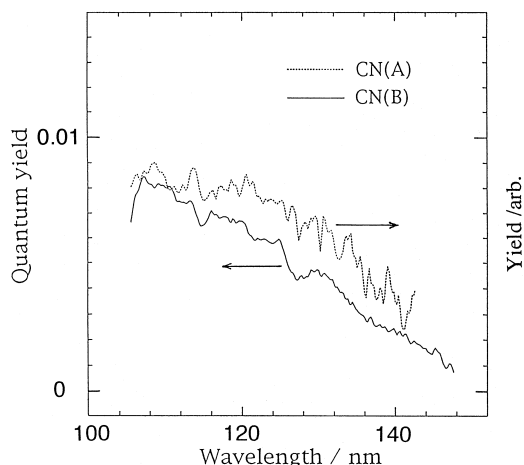


Fig. 3. Quantum yields for CN(B) and CN(A) formation in the VUV photodissociation of $\text{CH}_2(\text{CN})_2$ vs. wavelength of the exciting light.

Fig. 3 shows the fluorescence quantum yields calculated as the ratios of the CN(A,B) fluorescence excitation cross-sections to the absorption cross-section. The CN(B) quantum yield gives a maximum of 0.0085 at the highest energy end, i.e. at 107 nm. Due to the low response of our detection system (O54 + R955) in the IR region used to cover the full range of the broad banded CN(A–X) system, the absolute scale for the CN(A) quantum yield cannot be given here. We estimate, however, that the CN(A) quantum yield lies at the level as small as that of CN(B). The total quantum yield then amounts to $\approx 2\%$ at 107 nm, which is comparable with that observed for the VUV photolysis of CH_3CN [7,8]. Although the data in Fig. 3 are somewhat scattered, a close inspection reveals that these quantum yields generally show a monotonic increase with increasing excitation energy. No band exhibits prominent quantum yields, which indicates the presence of a specific excited state that strongly couples with dissociative excitation channels.

The fluorescence quantum yield is a measure of the interaction strength between the photoexcited state and dissociative state leading to the emitting species. The relatively monotonic variation in the quantum yield with the excitation wavelength and their low values clearly indicate that the photoexcited states do not directly correlate with the fluorescent surfaces and that the fluorescent decay channels are competitive with other non-radiative ones, which may dominate the quantum yield. The gradual increase in the quantum yield with increasing excess energy is also indicative of a near-statistical decay of the initial excited state into the lower states from which the reactions take place. Although no quantitative data on the non-radiative channels are available, it is likely that intramolecular electronic energy relaxation may be fast enough in the VUV energy region where excited states are congested so as to allow the competition between the dissociative excitation and other reactive channels. A low quantum yield ($\leq 2\%$) for the CN(A,B) formation and a similar monotonic increase are also observed in the VUV photolysis of CH_3CN [7,8]. The dissociative excitation steps, $\text{CH}_3\text{CN}^{**} \rightarrow \text{CH}_3 + \text{CN}(\text{B}, \text{A})$, have been found to compete with non-radiative reaction channel(s) from the observation of the kinetic hydrogen isotope effect showing the deuterium iso-

tope enhancement in the fluorescence quantum yields [7,8,22].

4. Concluding remarks

The photoabsorption bands of $\text{CH}_2(\text{CN})_2$ were assigned based on the term value consideration using the Rydberg formula. The Rydberg bands were ascribed to the transitions converging to the lowest four ionization limits ranging from 12.72 to 13.59 eV (Table 1). The vibrational progressions observed in the Rydberg bands were assigned to those of the CH_2 scissors $\nu_3(a_1)$ and CCC deformation $\nu_5(a_1)$ modes based on the equilibrium geometry calculations and vibrational frequency analysis for the Rydberg states. The quantum yields for the CN(A) and CN(B) formation were separately determined. The CN(B) quantum yield was found to be no greater than 1%; the CN(A) yield was estimated to have a similar magnitude. Their monotonic variation with the excitation wavelength indicates the absence of VUV photoexcited state that strongly couples with the dissociative excitation channels.

Acknowledgements

The authors are grateful to the staff of the UVSOR facility of IMS. We also thank the Information Processing Center of Hiroshima University for the allocation of CONVEX C-3210/C-3240 computer time. The present work was supported by the UVSOR Joint Research Program (1995–1996) of IMS.

References

- [1] For review, K. Shobatake, A. Hiraya, K. Tabayashi, T. Ibuki, in: Ed. C.Y. Ng, Vacuum Ultraviolet Photoionization and

- Photodissociation of Molecules and Clusters (World Scientific, Singapore, 1991) Ch. 11.
- [2] L.C. Lee, *J. Chem. Phys.* 72 (1980) 6414.
- [3] K. Kanda, S. Katsumata, T. Nagata, Y. Ozaki, T. Kondow, K. Kuchitsu, A. Hiraya, K. Shobatake, *Chem. Phys.* 175 (1993) 399.
- [4] For example, E.D. Poliakoff, S.H. Southworth, D.A. Shirley, K.H. Jackson, R.N. Zare, *Chem. Phys. Lett.*, 65 (1979) 407.
- [5] K. Kanda, S. Katsumata, T. Nagata, T. Kondow, A. Hiraya, K. Tabayashi, K. Shobatake, *Chem. Phys.* 218 (1997) 199.
- [6] M. Suto, L.C. Lee, *J. Geophys. Res.* 90 (1985) 13037.
- [7] K. Shobatake, S. Ohshima, A. Hiraya, Y. Matsumoto, K. Tabayashi, in: Intern. Conf. on Photochemistry, Tokyo, August, 1985, Book of Abst., p. 532.
- [8] M. Kono, Ph. D. Thesis, The Graduate University for Advanced Studies, Okazaki, 1995.
- [9] D.-C. Che, T. Kasai, M. Ohyama, K. Kuwata, M. Kono, K. Tabayashi, K. Shobatake, *Chem. Lett.* (1994) 133.
- [10] R. Rianda, R.P. Frueholz, A. Kuppermann, *J. Chem. Phys.* 80 (1984) 4035.
- [11] H. Stafast, H. Bock, *Z. Naturforsch., Teil B* 28 (1973) 746.
- [12] C.B. MacDonald, D.S. Waddell, N.P.C. Westwood, *J. Mol. Struct.* 162 (1987) 341.
- [13] M.J. Frisch, G.W. Trucks, M. Head-Gordon, P.M.W. Gill, M.W. Wong, J.B. Foresman, B.G. Johnson, H.B. Schlegel, M.A. Robb, E.S. Replogle, R. Gomperts, J.L. Andres, K. Raghavachari, J.S. Binkley, C. Gonzalez, R.L. Martin, D.J. Fox, D.J. DeFrees, J. Baker, J.J.P. Stewart, J.A. Pople, GAUSSIAN 92 (Gaussian, Pittsburgh, PA, 1992).
- [14] L.A. Curtiss, K. Raghavachari, G.W. Trucks, J.A. Pople, *J. Chem. Phys.*, 94 (1991) 7221 and references therein.
- [15] E. Hirota, Y. Morino, *Bull. Chem. Soc. Jpn.*, 33 (1960) 705 and references therein.
- [16] R. Cambi, W. von Niessen, *J. Electron Spectrosc. Rel. Phenom.* 42 (1987) 245.
- [17] M.B. Robin, *Higher Excited States of Polyatomic Molecules* (Academic, New York, 1975), Vol. 2.
- [18] C. Fridh, *J. Chem. Soc. Faraday Trans. II* 74 (1978) 2193.
- [19] W.J. Hehre, L. Radom, P.v.R. Schleyer, J.A. Pople, *Ab Initio Molecular Orbital Theory* (Wiley-Interscience, New York, 1986), p. 226ff.
- [20] D.J. DeFrees, A.D. Mclean, *J. Chem. Phys.* 82 (1985) 333.
- [21] K.P. Huber, G. Herzberg, *Molecular Spectra and Molecular Structure. IV. Constants of Diatomic Molecules* (Van Nostrand, New York, 1979).
- [22] K. Tabayashi, K. Shobatake, *J. Chem. Phys.* 87 (1987) 2404.